Investigating Correlations and Calibration of SMAP-Sentinel L2 and In-situ Soil Moisture in Thailand

Apiniti Jotisankasa , Kritanai Torsri * , Soravis Supavetch , Kajornsak Sirirodwattanakool , Nuttasit Thonglert , Rati Sawangwattanaphaibun , Apiwat Faikrua , Pattarapoom Peangta , Jakrapop Akaranee

Posted Date: 6 September 2023

doi: 10.20944/preprints202309.0289.v1

Keywords: soil moisture; remote sensing; SMAP; Sentinel-1; soil-water retention curve; validation; Thailand

Article

Investigating Correlations and Calibration of SMAP-Sentinel L2 and In-situ Soil Moisture in Thailand

Apiniti Jotisankasa [1], Kritanai Torsri [2,*], Soravis Supavetch [1], Kajornsak Sirirodwattanakool [3], Nuttasit Thonglert [3], Rati Sawangwattanaphaibun [2], Apiwat Faikrua [2], Pattarapoom Peangta [2] and Jakrapop Akaranee [2]

[1] Department of Civil Engineering, Faculty of Engineering, Kasetsart University, Bangkok, Thailand, 10900; fengatj@ku.ac.th; fengsvsu@ku.ac.th

[2] Hydro-Informatics Innovation Division, Hydro-Informatics Institute, Ministry of Higher Education, Science, Research and Innovation, Bangkok, Thailand, 10900; rati@hii.or.th; apiwat@hii.or.th; pattarapoom@hii.or.th; jakrapop@hii.or.th

[3] formerly, Department of Civil Engineering, Faculty of Engineering, Kasetsart University, Bangkok, Thailand, 10900; kajornsak.si@ku.th; nuttasit.t@ku.th

* Correspondence: kritanai@hii.or.th

Abstract: Soil moisture plays a crucial role in various hydrological processes and energy partitioning of the global surface. The Soil Moisture Active Passive-Sentinel (SMAP-Sentinel) remote sensing technology has demonstrated a great potential in monitoring soil moisture at a scale greater than 1 km. This capability can be applied to improve weather forecast accuracy, enhance water management for agriculture, and climate-related disasters. Despite the techniques increasing used worldwide, its accuracy still requires field validation in specific regions like Thailand. In this paper, we report on extensive in-situ monitoring of soil moisture (from surface up to 1 m depth) at 10 stations across Thailand spanning the years 2021 to 2023. The aim was to validate SMAP surface soil moisture (SSM) Level 2 product over a period of two years. Using one month averaging approach, the study revealed linear relationships between the two measurement types, with the coefficient of determination (R-squared) varying from 0.13 to 0.58. Notably, areas with more uniform land use and topography such as croplands tended to have a better coefficient of determination. We also conducted detailed soil core characterization, including soil-water retention curves, permeability, porosity, and other physics properties. These soil properties were then used for estimating the correlation constants between SMAP and in-situ soil moistures using multiple linear regression. The results demonstrated R-squared values between 0.933 and 0.847. An upscaling approach of SMAP was proposed which showed a promising results when using 3-month average of all measurements in cropland together. The finding also suggest that the SMAP-Sentinel remote sensing technology exhibits significant potential for accurate soil moisture monitoring in diverse applications. Further validation efforts and research, particularly in terms of root zone depths and area-based assessments, especially in the agricultural sector, can greatly improve the technology's effectiveness and usefulness in the region.

Keywords: soil moisture; remote sensing; SMAP; Sentinel-1; soil-water retention curve; validation; Thailand

1. Introduction

Soil moisture is a critical factor in various fields of hydrology, agriculture, climate modeling, and land management. The temporal and spatial distribution of soil moisture in watersheds can affect the amount of water that enters streams, rivers, and groundwater, which in turn can impact water availability for human consumption, agriculture, and other uses [1]. A wise management of soil moisture is thus critical for ensuring sustainable land use and maximizing agricultural productivity. Soil moisture data can be used to provide information about plant growth and health, nutrient availability, soil erodibility, as well as to optimize the irrigation schedule and to aid in crop selection.

 doi:10.20944/preprints202309.0289.v1

Additionally, soil moisture is an important parameter in predicting climate-related disasters such as flood, landslide and drought. Early warning systems for such disasters often rely on accurate soil moisture monitoring as part of their scheme.

As soil moisture significantly affects the partitioning of energy at the land surface, it exerts a considerable impact on the surface energy balance and atmospheric processes, such as surface temperature, surface evaporation, and transpiration. Knowledge of soil moisture can enhance accuracy of weather forecasting and climate modeling on both global and regional scales. Remote sensing techniques have been developed to measure soil moisture and related parameters [2], such as active and passive microwave remote sensing (e.g., Soil Moisture Active Passive, known as SMAP [3]), optical remote sensing for Normalized Difference Vegetation Index (NDVI), and thermal remote sensing (Moderate Resolution Imaging Spectroradiometer (MODIS) or the Thermal Infrared Sensor (TIRS).

SMAP is a NASA satellite mission launched in 2015, utilizing both active and passive microwave remote sensing to measure soil moisture with high spatial resolution [3]. Other satellites, such as Soil Moisture and Ocean Salinity (SMOS)), also employ passive microwave techniques, particularly at L-band frequency, enabling global mapping of near-surface (0–5 cm) soil moisture with 25 to 40 km spatial resolution and temporal resolution of 2 to 3 days [2]. A study by Forgotson et al. [4] demonstrated several applications of SMAP soil moisture products to improve soil moisture-related monitoring and early warning systems in the United States (U.S.) through case studies. By utilizing the SMAP level 4 products and model-driven soil moisture data, Forgotson et al. [4] successfully mapped most of the recent flooded areas in the U.S., though with some degree of overestimation due to the coarse spatial resolution of SMAP.

To assess the reliability of the SMAP L4 product, Rahman et al. [5] conducted a validation analysis of the SMAP soil moisture (SSM) data against in-situ measurements obtained across various locations and land use types in the U.S. The authors suggested that SMAP L4 data can be a valuable tool for accurately mapping cropland inundation, providing useful information for flood monitoring and management. The study revealed that the SMAP data demonstrated the closest agreement with in-situ measurements over the central Great Plains and cultivated crops throughout the year. In a study conducted by Zhang et al. [6], the reliability of SMAP L-band radiometer data was also validated against in-situ soil moisture data at selected agriculture sites in the U.S. The previous study specifically focused on assessing the influence of spatial-temporal characteristics, particular on land covers such as Cultivated Crops, Deciduous/Evergreen Forest, and Pasture/Hay. Their work also explained a methodology to derive soil wetness index from the time-series of SMAP L-band brightness temperatures. The finding of their study indicated that the SMAP L4 products exhibited high reliability and demonstrated a significant impact of spatial-temporal characteristics, particularly in certain land cover types. In addition, the SMAP L4 soil moisture data was found to be significantly affected by seasonal variation in these land covers.

These previous studies clearly demonstrate the importance of regional and local validation of the SSM data prior to its application in any specific region worldwide. Such validation is essential to ascertain the reliability and suitability of the SSM data for use in particular geographical areas. This current study thus aims at validating the SSM products for Thailand by correlating the remote sensing data with in-situ soil moisture measurements from 10 telemetry stations, encompassing diverse soil types in Thailand. In addition, a detailed analysis of soil properties, including particle size distribution, plasticity, organic content, thermal conductivity, porosity and soil-water characteristic curves, was also conducted. These analyses were subsequently used in multiple linear regression analysis to provide preliminary transfer functions for remote sensing and in-situ soil moisture measurements.

In the paper, Section 2 provides a detailed description of the material and methods employed in this study. Subsequently, in Section 3, we present the analysis results derived from in-situ measurements and validation of the SMAP soil moisture. Finally, Section 4 provide a comprehensive discussion of the results and summarize the main findings obtained from this study.

2. Materials and Methods

 doi:10.20944/preprints202309.0289.v1

2.1. Remote sensing soil moisture

This study utilizes the SMAP radiometer/Copernicus Sentinel-1 soil moisture product (L2_SM_SP), designated as SPL2SMAP_S SMAP/Sentinel-1 L2 Radiometer/Radar 30-Second Scene 3-km EASE-Grid Soil Moisture, Version 3 [7, 8]. Being a Level-2 (L2) soil moisture product, it provides estimates of land surface conditions retrieved by both the SMAP radiometer during 6:00 a.m. descending and 6:00 p.m. ascending half-orbit passes and the Sentinel-1A and -1B radar. The soil moisture data was derived using SMAP L-band brightness temperatures and Copernicus Sentinel-1 C-band backscatter coefficients. Subsequently, the datasets were resampled to an Earth-fixed, cylindrical 3-km Equal-Area Scalable Earth Grid, Version 2.0 (EASE-Grid 2.0) [7, 8]. For Thailand, the available SMAP L-band data mostly corresponds to nighttime, while the Sentinel-1 data covers both daytime and nighttime observations. In this study, the soil moisture data from 149 files spanning approximately one month are stitched together to cover all pixels across Thailand. An example of the monthly soil moisture map that can be produced is shown in Figure 1.

2.2. In-situ soil moisture monitoring

In-situ soil moisture data used to validate the SMAP soil moisture were collected from 10 telemetry monitoring stations installed throughout various locations in Thailand. These stations were extensions of the existing telemetry weather stations belonging to the Hydro-Informatics Institute (HII) of Thailand. The locations of these stations were carefully selected to represent a variety of soil types, geographical features, and climate conditions in Thailand, offering valuable data for understanding soil moisture behavior in more topographically varied landscapes.

The distribution of the monitoring stations across diverse topographic and land-use settings in Thailand is presented in Figure 1 and summarized in Table 1. As seen, five stations (HNKA, WGYG, VLGE50, BNKE, and THAT) were situated on flat plains, while three stations (KKCN, PAII, and SWR036) were located in hilly terrains, and the other two stations (VLGE49 and NMUB) were on undulating plains.

From Table 1, the telemetry stations exhibited a wide variation in annual rainfall, ranging from the lowest recorded value of 983.0 mm (KKCN station) to the highest recorded value of 2386.0 mm (SWR036 station). This rainfall variability reflects the diverse hydrological conditions across the monitored regions and can significantly influence soil moisture patterns. Moreover, the land use types surrounding these stations encompassed various categories, including agriculture (field crops or rice paddy), perennial, urban areas, and forested regions. Understanding soil moisture features in these distinct land use types is also essential for assessing the impacts of different land covers on soil moisture dynamics.

Preprints (www.preprints.org) | NOT PEER-REVIEWED | Posted: 6 September 2023 doi:10.20944/preprints202309.0289.v1

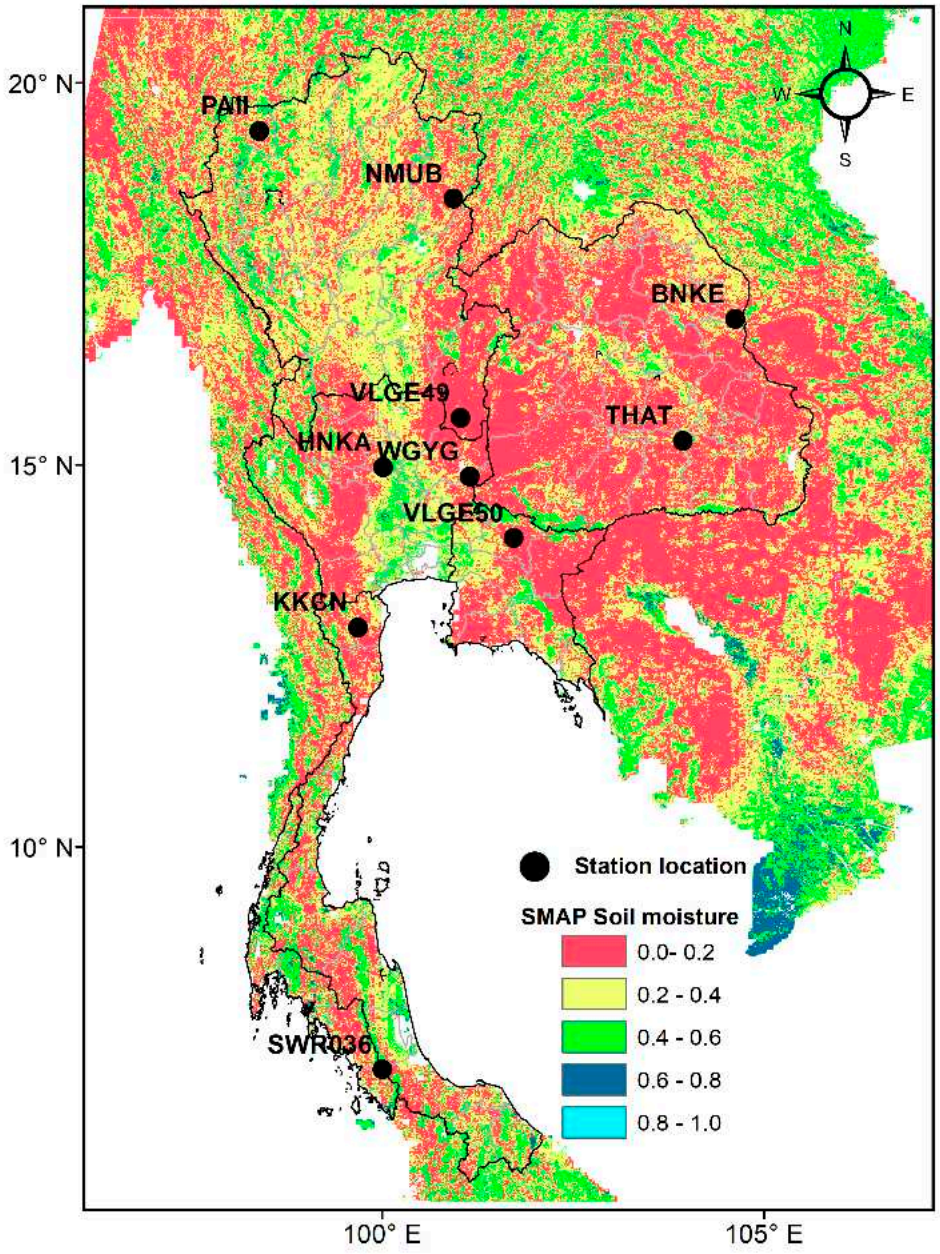

Figure 1. An example of a typical SMAP soil moisture map (shaded color) and locations of in-situ soil moisture stations (black circles) used in the study.

Table 1. Location details of telemetry weather/soil moisture stations used in this study.

No.	Station name	Province	Latitude	Longitude	Landuse[1]	Geology[2]	Geography	Elevation (AMSL)	Average annual rainfall[3]
1	KKCN	Phetchaburi	12.8723	99.6835	Perennial plant	Sedimentary and metamorphic	Plain at the foot of hilly terrains	64 m	983.0 mm
2	VLGE49	Phetchabun	15.61636	101.023	Field crop	Quaternary sediment	Undulating plain	96 m	1210.0 mm
3	HNKA	Chai Nat	14.9696	100.0104	Rice paddy	Quaternary alluvial sediment	Flood plain	13 m	1010.8 mm
4	WGYG	Saraburi	14.8481	101.1459	Field crop	Sedimentary rock	Plain	93 m	1185.2 mm
5	VLGE50	Prachinburi	14.0426	101.7204	Rice paddy	Quaternary alluvial sediment	Alluvial plain	27 m	1762.4 mm
6	NMUB	Nan	18.48421	100.93071	Forest	Sedimentary rock	Undulating plain	333 m	1238.9 mm
7	PAII	Mae Hong Son	19.37012	98.39309	Fruit trees	Granitic	Plain between complex mountain ranges	776 m	1315.8 mm
8	BNKE	Nakhon Phanom	16.90888	104.6187	Rice paddy	Sedimentary and metamorphic	Plain	153 m	2328.0 mm
9	THAT	Surin	15.31667	103.9355	Urban	Sedimentary rock	Plain	128 m	1445.3 mm
10	SWR036	Satun	7.08837	100.002	Perennial plant	Igneous	Basin surrounded by hills	110 m	2386.0 mm

[1] based on land use map of Land Development Department, Thailand, [2] based on geology map of Department of Mineral Resources, Thailand, [3] based on Thai Meteorological Department.

doi:10.20944/preprints202309.0289.v1

Preprints (www.preprints.org) | NOT PEER-REVIEWED | Posted: 6 September 2023 doi:10.20944/preprints202309.0289.v1

To delineate the soil stratigraphy within the uppermost 1-meter layer at the monitoring station, a test pit was dug to collect in-situ soil samples (both disturbed and undisturbed samples) for further testing. In-situ field classification was performed based on soil color and texture, enabling the description of soil stratigraphy, which was divided into 2–3 layers over the 1-m depth. The soil moisture sensors (MAS-1, METER Group, with a standard 2-wire, 4- to 20-mA type) were installed at depths of 0.10, 0.30, 0.60 and 1.00 meter along the side wall of the pit, as shown in Figure 2. During the sensor installation process, each sensor was horizontally inserted into a pre-bored hole created on the test pit side-wall using a dummy sensor of the same size to minimize any potential damage to the actual sensor. Great care was taken to minimize soil disturbance during installation. However, when the soil was dry and compacted, a small hole (1–2 cm in diameter and about 10 cm long) was created horizontally into the test pit wall. The excavated soil was then moistened and carefully backfilled into the hole before inserting the sensor. Following the installation of all sensors on the pit wall, the pit was backfilled with excavated soil to restore it to its original condition.

The MAS-1 sensor employs capacitance/frequency domain technology to determines local volumetric water content (θ) by measuring the soil's dielectric constant. In this study, the volumetric water content obtained from the in-situ sensor is referred to as the local water content (θ), while the water content derived from remote sensing is called SMAP surface soil moisture content (SSM). For site-specific calibration of the soil moisture sensors, soil samples were collected from each delineated soil layer. Undisturbed soil samples were collected using a soil core sampler (63 mm inner diameter) from each soil layer to determine porosity, soil-water retention curve, hydraulic conductivity, and thermal conductivity. Disturbed soil samples were used for basic classification tests, such as organic content, wet sieve analysis, hydrometer test, specific gravity and Atterberg's limits.

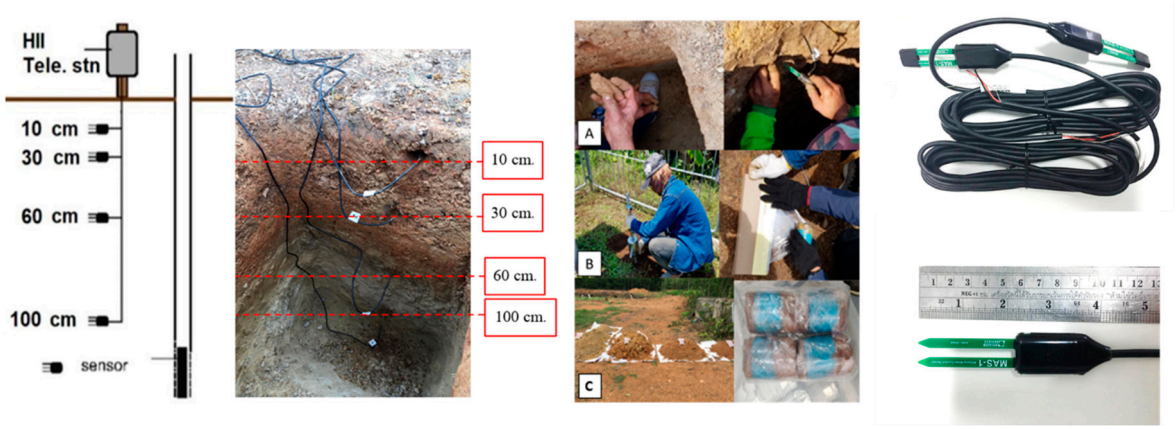

Figure 2. Test pit and installation of soil moistures sensor.

2.3. Laboratory testing of soil

Figure 3 shows the calibration box (with the inner dimension of 16.2×18.2×20.1 cm^3) and the procedure used to establish the relationship between the sensor output (mA) and volumetric water content ($\theta = V_w/V$, where V_w is the volume of water and V is the total volume of soil). This specific size of the calibration box was chosen to minimize boundary effect on the moisture sensor signal, as suggested in Suwansawat et al. [9]. To replicate field conditions as closely as possible, the soil sample was re-compacted in the calibration box to achieve the same dry unit weight as that of undisturbed sample. A number of soil samples were compacted to different moisture contents and the sensor output was measured accordingly for each moisture level. The final stage of calibration involved soaking the samples for several days until the sensor reading stabilized, indicating a saturated condition.

Preprints (www.preprints.org) | NOT PEER-REVIEWED | Posted: 6 September 2023 doi:10.20944/preprints202309.0289.v1

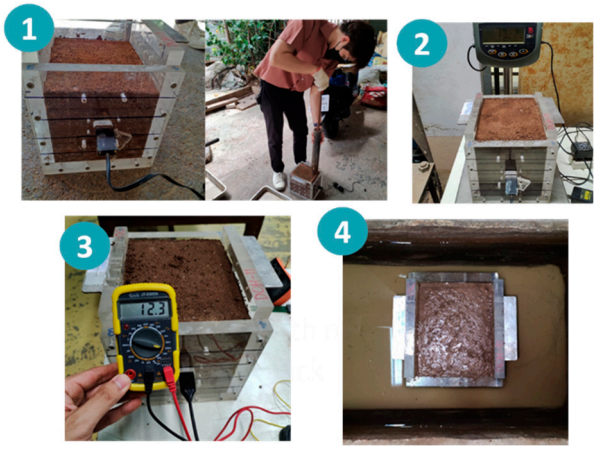

Figure 3. Calibration process for soil moistures sensor: (1) sample preparation, (2) sample weighing, (3) Sensor reading at different compaction moisture contents and (4) Final soaking.

Three undisturbed cylindrical samples (63 mm in diameter and about 25 mm in height) were obtained from each soil layer and utilized for conducting soil-water retention curve, hydraulic conductivity and thermal conductivity tests. The soil-water retention curve (SWRC) procedure involved measuring soil suctions at different water contents in a drying path, as explained in Barus et al. [10] and Shrestha et al. [11]. The test began by soaking the soil sample for several days to reach full saturation and then gradually drying the sample. At each drying stage, the soil suction, weight, and dimension of the soil sample were measured under equilibrium condition. For suction measurements, three methods were employed, namely, the miniature tensiometer for matric suctions less than 100 kPa, the pressure plate for matric suctions between 200 to 1500 kPa, and the isopiestic technique (salt solution equilibrium) for total suctions greater than 1500 kPa. Additionally, porosity and volume changes of the soil sample were also monitored during the SWRC test. The hydraulic conductivity and thermal conductivity tests were carried out on the undisturbed samples in a saturated condition following American Society for Testing and Materials (ASTM) standards as described in [12] and [13], respectively. Other index properties, including wet sieve analysis, hydrometer test, specific gravity and Atterberg's limits were determined based on the ASTM standards [14–16]. The organic content was determined using chronic acid titration method [17].

3. Results

Table 2 summarizes the basic soil properties and soil classification (based on the unified soil classification system, USCS) of all prescribed soil layers in all telemetry stations. At four stations (KKCN, VLGE49, VLGE50, PAII) the soils were described as clays (CL and CH) of varying plasticity indices (PI) ranging between 5.7 to 37.9. Silty soils (classified as ML and MH) were found at 3 stations, namely, WGYG, NMUB, and PAII. Silty sands and clayey sands were present at the remaining 4 stations, i.e., HNKA, BNKE, THAT, SWR036. The organic contents of the soils in most cases were lower than 20 g/kg which was considered as low, with an exception of WGYG (0–50 cm) and PAII (0–10 cm) which had higher organic matter varying between 30 to 35 g/kg.

The porosity of HNKA and THAT soils were relatively lower than the others (< 0.35) which indicated the compaction of the soil that resulted from human activities, e.g., preparation of the land for urban uses or any other development. It should also be noted that at HNKA station, the soil collected at the telemetry station was classified as clayey sand and silty sand, while the soil map of Land Development Department (LDD) of Thailand indicated that soil in the area should be clay (Unit 4, Cn). This discrepancy was due to the fact that the soil moisture sensors were required to be installed near the telemetry station which was located on an engineering sandy soil fill and may not be representative of the clay that extended in most of nearby rice paddy. Such discrepancy between the properties of collected soil and the information from LDD soil map was to be expected, due to spatial variability of the in-situ soil.

Table 2. Basic soil properties collected from 10 telemetry stations.

No	Station name	Depth (cm)	Atterberg limits			Grain size distribution (%)				Porosity	Organic content (g/kg)	Specific gravity	Soil type (Unified Soil Classification System)
			Liquid Limits (%)	Plastic Limits (%)	Plasticity Index, PI	Gravel	Sand	Silt	Clay				
1	KKCN	0-50	44.70	24.62	20.08	4.24	27.90	21.04	46.83	0.41	20.0	2.64	CL
		50-100	52.80	30.83	21.97	0.71	23.16	26.22	49.91	0.47	5.8	2.41	CH
2	VLGE49	0-100	43.82	25.12	18.70	0.88	37.19	2.03	59.90	0.54	19.0	2.70	CL
3	HNKA	0-10	33.40	18.52	14.88	11.70	66.56	8.29	13.45	0.39	10.0	2.59	SC
		10-40	24.10	14.51	9.59	11.39	43.52	23.29	21.81	0.37	6.8	2.52	SM
		40-100	NP	NP	NP	2.05	63.01	16.87	18.07	0.49	4.9	2.63	SC
4	WGYG	0-50	62.00	48.38	21.63	7.17	40.11	41.49	11.23	0.57	30.0	2.68	MH
		50-100	39.80	29.03	10.77	4.55	44.31	45.44	5.70	0.52	5.8	2.64	ML
5	VLGE50	0-20	25.90	20.16	5.74	2.03	45.73	2.15	50.09	0.45	11.0	2.69	CL
		20-100	29.70	20.79	8.91	3.83	39.61	5.46	51.10	0.38	1.8	2.70	CL
6	NMUB	0-100	NP	NP	NP	17.53	32.04	40.43	10.00	0.58	17.0	2.65	ML
7	PAII	0-10	39.00	28.91	10.09	5.76	43.42	44.32	6.50	0.68	35.0	2.67	ML
		10-100	64.30	26.39	37.91	0.22	43.57	4.20	52.01	0.55	3.5	2.71	CH
8	BNKE	0-50	NP	NP	NP	18.89	46.24	22.26	12.61	0.41	15.0	2.60	SM
		50-70	NP	NP	NP	14.92	50.03	22.13	12.92	0.36	5.8	2.52	SM
		70-100	24.20	16.75	7.45	7.75	48.92	20.80	22.53	0.38	5.3	2.62	SM
9	THAT	0-10	NP	NP	NP	8.19	55.32	15.06	21.44	0.36	10.0	2.60	SC
		10-100	NP	NP	NP	0.07	70.21	13.97	15.74	0.35	0.8	2.49	SM
10	SWR036	0-10	NP	NP	NP	0.25	70.04	16.05	13.66	0.52	15.0	2.55	SM
		10-40	NP	NP	NP	1.46	70.41	12.92	15.22	0.42	8.0	2.48	SC
		40-100	NP	NP	NP	7.51	82.25	4.66	5.57	0.44	1.8	2.60	SP

NP= Non-plastic.

doi:10.20944/preprints202309.0289.v1

Preprints (www.preprints.org) | NOT PEER-REVIEWED | Posted: 6 September 2023 doi:10.20944/preprints202309.0289.v1

3.1. Soil moisture sensor calibration

The soil moisture sensor required a soil-specific calibration in order that reliable reading can be achieved. Figure 4 shows some examples of sensor calibration results for different soil types. Table 2 summarizes the coefficients of the calibration equation for soil moisture sensor which takes a linear form as follows.

$$\theta = ax + b \tag{1}$$

Where x is the sensor reading in milliamp (mA), a and b are the fitting parameters from linear regression and θ is the volumetric water content (%). The coefficient of determination, R^2, also summarized in Table 2, was found to range between 0.980 to 0.999, which indicated a satisfactory correlation and accuracy. It is noteworthy that the default calibration equation provided by the manufacturer of the MAS-1 sensor can give very different values of soil moisture than the soil-specific equation (Table 2) by about 7% (in terms of θ) on average and the maximum discrepancy in θ can be as much as 22.9%. It is thus of utmost importance to determine the soil-specific calibration equation in the laboratory using the in-situ soil for reliable measurement.

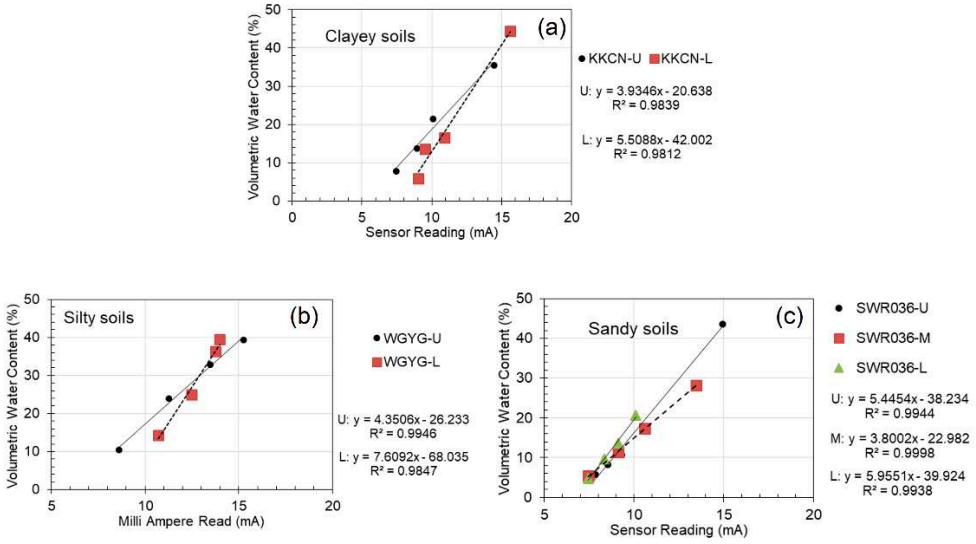

Figure 4. Examples of sensor calibration equations for different soil types: (a) clayey soils,(b) silty soils, and (c) sandy soils.

In this study, multiple linear regression analyses were conducted to model the relationships between the fitting parameters (a and b, taken as dependent variables) and soil properties (taken as independent variables), as shown in Equations (2) and (3).

$$a = \alpha_c + \alpha_1 X_1 + \alpha_2 X_2 + \alpha_3 X_3 + \alpha_4 X_4 + \alpha_5 X_5 + \alpha_6 X_6 + \alpha_7 X_7 \tag{2}$$

$$b = \beta_c + \beta_1 X_1 + \beta_2 X_2 + \beta_3 X_3 + \beta_4 X_4 + \beta_5 X_5 + \beta_6 X_6 + \beta_7 X_7 \tag{3}$$

Where X_1 is the plasticity index (for non-plastic soil, X_1 is taken as zero), X_2 is the % gravel, X_3 is the % sand, X_4 is the % silt, X_5 is the % clay, X_6 is the porosity (unitless) and X_7 is the organic content (g/kg) as summarized in Table 3. The fitting parameters, α_i and β_i ($i = 1, 2, \ldots, 7$) are obtained from multiple linear regression analysis as summarized in Table 4. These relationships are useful in case there is no site-specific sensor calibration test and only the information on soil texture, porosity and organic contents are available. Then the sensor calibration coefficients (a and b) can be predicted using the known basic soil properties $(X_1, \ldots, X_7)$. The coefficient of determination ($R^{2)}$ from the multiple linear regression analysis of a and b parameter was 0.748 and 0.721 respectively.

Table 3. Moisture sensor calibration coefficients, hydraulic and thermal properties of soils.

No	Station name	Soil unit*	Depth (cm)	Sensor calibration coefficients			Hydraulic conductivity, k, cm/s	Thermal conductivity, , W/(m.K)
				a	b	R^2		
1	KKCN	U	0–50	3.9346	-20.638	0.9839	9.44E-05	1.76
		L	50–100	5.5088	-42.002	0.9812	1.32E-04	2.34
2	VLGE49	-	0–100	4.9995	-30.271	0.9822	3.31E-05	1.68
3	HNKA	U	0–10	3.6222	-22.539	0.9802	1.80E-07	1.41
		M	10–40	4.1060	-26.655	0.9872	1.18E-07	1.76
		L	40–100	3.6185	-19.873	0.9940	5.83E-04	2.01
4	WGYG	U	0–50	4.3506	-26.233	0.9946	2.56E-04	1.44
		L	50–100	7.6092	-68.035	0.9847	1.68E-04	1.26
5	VLGE50	U	0–20	4.4931	-27.202	0.9911	1.02E-07	1.44
		L	20–100	3.5044	-18.562	0.9915	2.61E-07	2.01
6	NMUB	-	0–100	6.8022	-56.189	0.9910	2.20E-03	1.31
7	PAII	U	0–10	8.2213	-63.759	0.9846	1.33E-03	2.63
		L	10–100	6.1297	-38.391	0.9911	2.80E-06	1.13
8	BNKE	U	0–50	4.8077	-37.689	0.9947	8.04E-05	1.48
		M	50-70	3.5852	-22.114	0.9921	2.56E-06	1.67
		L	70-100	4.2354	-29.708	0.9911	4.21E-07	2.51
9	THAT	U	0-10	3.5023	-24.270	0.9940	1.62E-06	2.87
		L	10-100	3.4499	-22.674	0.9872	1.66E-05	2.89
10	SWR036	U	0-10	5.4454	-38.234	0.9944	1.93E-03	0.88
		M	10-40	3.8002	-22.982	0.9998	4.32E-03	2.34
		L	40-100	5.9551	-39.924	0.9938	4.20E-03	1.26

* U= Upper; M = Middle; L= Lower.

doi:10.20944/preprints202309.0289.v1

Preprints (www.preprints.org) | NOT PEER-REVIEWED | Posted: 6 September 2023 doi:10.20944/preprints202309.0289.v1

Table 4. Multiple linear regression coefficients for predicting the sensor calibration equations using soil properties.

α_c	α_1	α_2	α_3	α_4	α_5	α_6	α_7
1598.835	–0.000552	–15.971	–16.009	–15.985	–16.007	14.960	–0.0608
β_c	β_1	β_2	β_3	β_4	β_5	β_6	β_7
–16579.396	0.123	165.669	166.105	165.639	166.058	–132.139	0.727

3.2. Hydraulic and thermal properties

Figure 5 illustrates the hydraulic conductivity values of the undisturbed core samples categorized by soil textures, ranging from fine-grained (CH) to coarse-grained (SP). The initials are shown according to the Unified Soil Classification System (CH = high-plasticity clay, CL = low-plasticity clay, MH = high-plasticity silt, ML = low-plasticity silt, SC = clayey sand, SM = silty sand and SP = poorly graded sand). The variation of hydraulic conductivity for the clay soils (CH and CL) ranged between 10^{-7} to 10^{-4} cm/s (about three order of magnitude), while that of silts (ML and MH) were between 10^{-4} to 10^{-3} cm/s (one order of magnitude). The upper range of the hydraulic conductivity of clay was relatively high (10^{-4} cm/s) due to the aggregated structure of the material. The clayey and silty sands (SC and SM) had hydraulic conductivities that varied to a greater extent, between 10^{-7} to 10^{-3} cm/s, which reflected the influence of clay particles presented. The poorly graded sand (SP) had the highest value of hydraulic conductivity of 4.2×10^{-3} cm/s. The observed variations in hydraulic conductivities clearly indicate that soil textures alone are insufficient to fully explain the range of hydraulic conductivities.

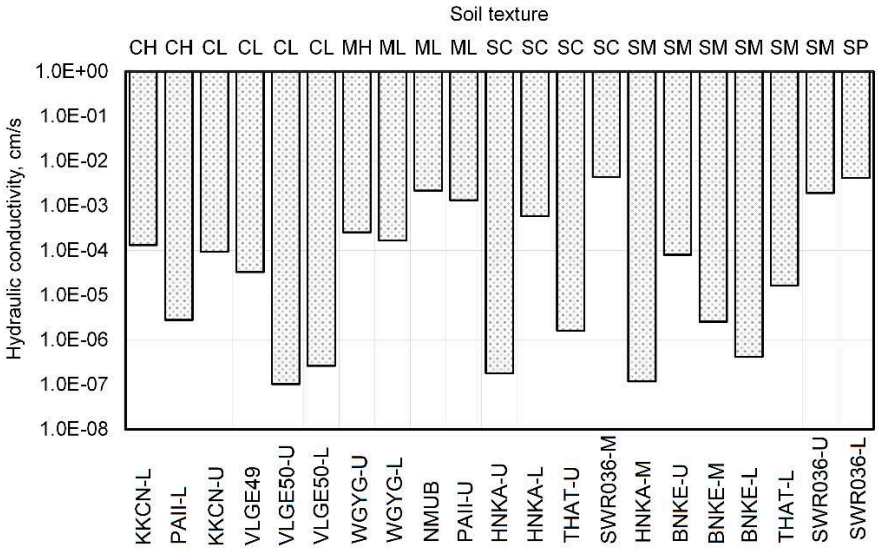

Figure 5. Hydraulic conductivity of the undisturbed core sample in a station and its soil texture's characteristics.

Figure 6 shows the thermal conductivity (λ) values of the undisturbed core samples by soil textures. The values of λ ranged from 0.88 to 2.89 W/(m.K), which is within the typical range observed for soils. Various factors, such as soil mineral, porosity, moisture content and organic content, can directly influence the thermal conductivity of the soil [18]. Notably, soils with higher quartz content are normally of greater thermal conductivities. Three soils, namely PAII-U, THAT-U, and THAT-L, exhibit thermal conductivities greater than 2.5 W/(m.K) and can be classified as silty (ML), sandy (SC), and sandy (SM) soils, respectively. It is likely that these soils have a higher proportion of quartz in their composition. However, it is important to note that there has been no mineral composition test conducted to verify this assumption.

Preprints (www.preprints.org) | NOT PEER-REVIEWED | Posted: 6 September 2023 doi:10.20944/preprints202309.0289.v1

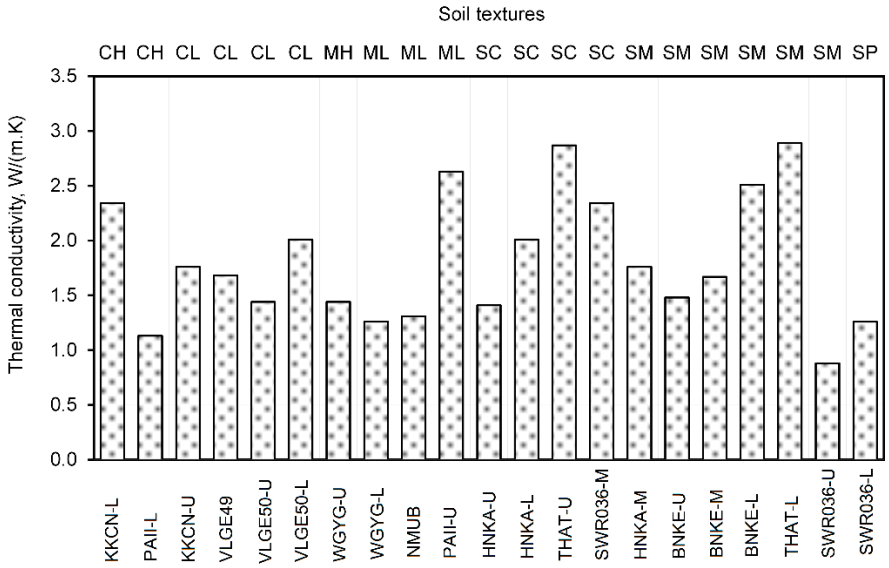

Figure 6. Thermal conductivity of the undisturbed core sample in saturated condition of a station and its soil texture's characteristics.

3.3. Soil-water retention curves

Soil-water retention curves (SWRC) of all the soils in this study are shown in Figure 7. It is noted that the curves represent drying path followed by the soil samples. These SWRCs were plotted as volumetric water content, θ (%) against suction, s (kPa) together with the curve fitting using Van Genuchten [19] model as shown in Equation (4).

$$\theta = (\theta_s - \theta_r)[\frac{1}{1+(p\cdot s)^n}]^m + \theta_r \quad (4)$$

Where θ_s is the saturated volumetric water content, θ_r is the residual volumetric water content, p is the fitting parameter inversely proportional to the air-entry suction of the soil, m and n are fitting parameters related to pore-size distribution. Table 5 summarizes the Van Genuchten parameters obtained from best fitting of the experimental data points for all soils tested in this study. The wide range of SWRC fitting parameters in this study is attributed to the diverse range of soils encountered. These parameters provide indications about various soil properties such as pore-size distribution, soil texture, soil aggregation structure, and organic content. It is important to note that these properties can vary spatially with depth and temporally, depending on the land-use type.

Table 5. Soil-water retention parameters estimated for 10 telemetry stations.

No	Station name	Soil unit*	Depth (cm)	Van Genuchten parameter					
				θ_s (%)	θ_r (%)	p (kPa^{-1})	n	m	R^2
1	KKCN	U	0–50	41	10	0.072	0.442	1.066	0.958
		L	50–100	47	10	0.496	0.560	1.026	0.960
2	VLGE49	-	0–100	54	20	0.00470	0.318	1.059	0.985
3	HNKA	U	0–10	39	7	0.0524	0.532	1.590	0.948
		M	10–40	37	3	0.00905	0.512	1.350	0.950
		L	40–100	49	2	0.0364	0.413	1.105	0.973
4	WGYG	U	0–50	57	19	0.0211	0.378	1.345	0.969
		L	50–100	52	5	0.0258	0.428	1.207	0.954
5	VLGE50	U	0–20	45	10	0.00216	0.356	1.114	0.962
		L	20–100	38	12	0.0189	0.394	1.168	0.957
6	NMUB	-	0–100	31	2	0.000843	0.484	1.504	0.975
7	PAII	U	0–10	31	15	0.0113	0.906	1.501	0.982
		L	10–100	46	18	0.0370	0.913	0.318	0.936
8	BNKE	U	0–50	30	17	0.00903	0.691	1.758	0.937
		M	50–70	26	6	0.158	0.938	0.309	0.996
		L	70–100	30	9	0.0806	1.075	0.308	0.981
9	THAT	U	0–10	36	6	0.360	4.556	0.0670	0.984
		L	10–100	35	0	0.00311	0.380	1.892	0.971
10	SWR036	U	0–10	17	2	0.164	20.779	0.0181	0.966
		M	10–40	30	0	0.00000133	0.347	17.014	0.989
		L	40–100	25	7	0.115	1.990	0.162	0.967

* U = Upper; M = Middle; L = Lower.

doi:10.20944/preprints202309.0289.v1

Preprints (www.preprints.org) | NOT PEER-REVIEWED | Posted: 6 September 2023 doi:10.20944/preprints202309.0289.v1

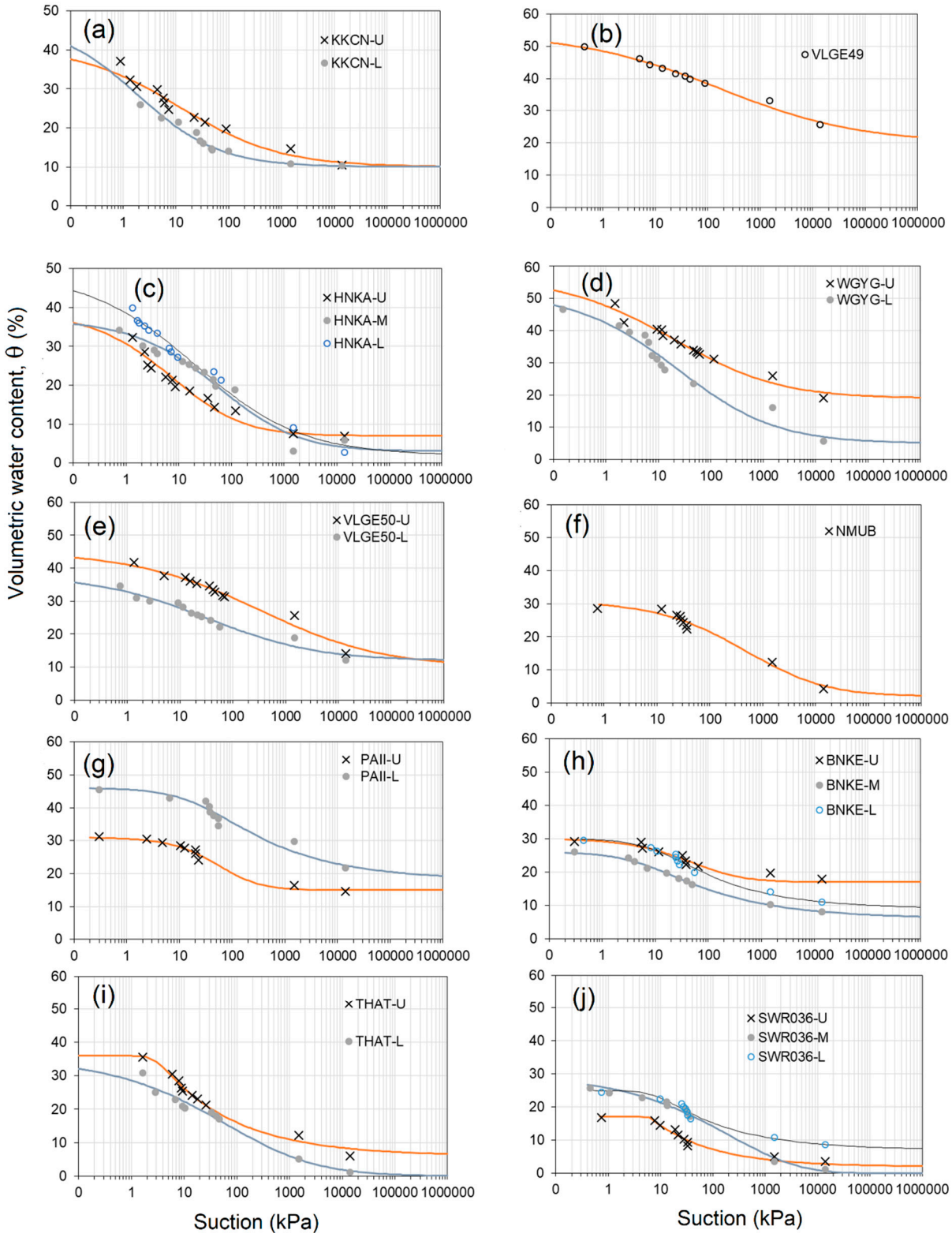

Figure 7. Soil water retention curves estimated for stations: (a) KKCN, (b) VLGE49, (c) HNKA, (d) WGYG, (e) VLGE50, (f) NMUB, (g) PAII, (h) BNKE, (i) THAT, and (j) SWR036 .

It is worth mentioning that hysteresis can significantly impact the SWRC. However, the parameters presented here solely pertain to the drying path, which involves increasing suction or decreasing water content. The wetting SWRC was not within the scope of this study and, therefore, not considered in the analysis. The drying SWRC is particularly relevant for analyzing drought events

 doi:10.20944/preprints202309.0289.v1

rather than flooding. By focusing on the drying path, these parameters can provide valuable insights into water availability and soil moisture retention during dry periods. However, for a comprehensive understanding of the soil-water relationship, it is important to investigate the wetting SWRC as well, which was not addressed in this particular study.

3.4. Correlations and Calibration of SMAP-Sentinel and In-situ Soil Moisture

3.4.1. Effect of temporal variation of soil moisture

The temporal resolution disparity between the SMAP product, which is available with intervals ranging from 3 to 8 days, and the high-frequency hourly measurements of in-situ moisture content necessitates the adoption of an averaging approach to establish correlations between these datasets. To elucidate this, Figures 8a and 9a vividly depict the original soil moisture variations at depths of 10 cm and 30 cm, respectively, for Station VLGE49. It is intriguing to observe that the SMAP soil moisture (SSM) exhibits significantly larger and more oscillatory amplitudes in comparison to in-situ readings. Particularly noteworthy is the observation that at a depth of 30 cm (as depicted in Figure 9), in-situ moisture values surpass those of SSM, suggesting the potential influence of diverse factors such as soil depth, interactions with groundwater, and spatial heterogeneity on the measurement outcomes.

Introducing a 1-month averaging methodology, as illustrated in Figures 8b and 9b, imparts a smoothing effect on the temporal profile of soil moisture, thereby attenuating the magnitude of fluctuations. This smoothing effect culminates in an advantageous enhancement of the correlation between the SMAP product and in-situ measurements, as discernible in Figures 10 and 11, depicting the relationship between soil moistures at depths of 10 cm and 30 cm, respectively. In subsequent analyses, the utilization of one-month average soil moisture predominantly guided the exploration of correlations between SSM and in-situ measurements.

Preprints (www.preprints.org) | NOT PEER-REVIEWED | Posted: 6 September 2023 doi:10.20944/preprints202309.0289.v1

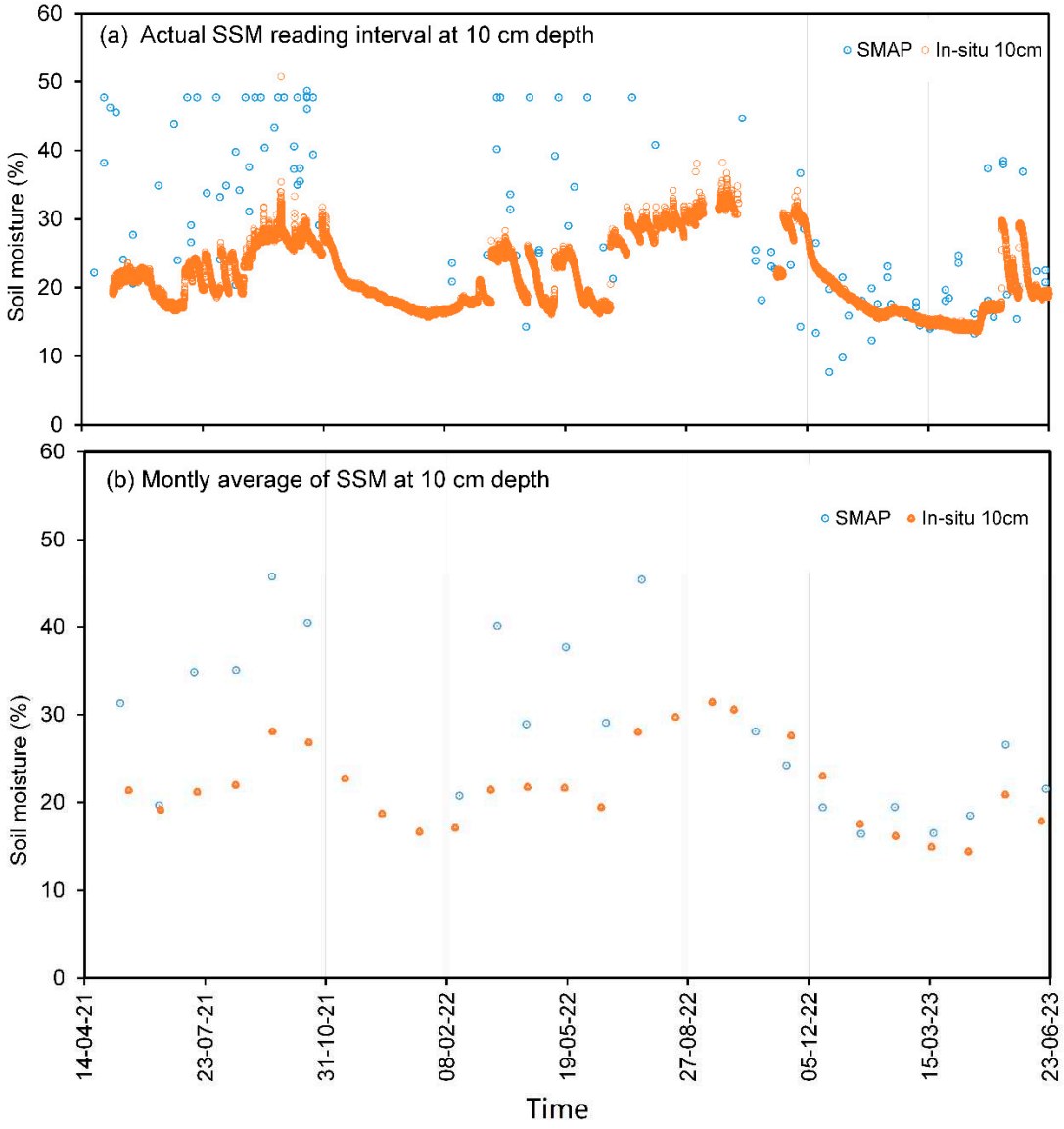

Figure 8. Variations of SMAP and in-situ soil moisture (10 cm depth) from Station VLGE49:(a) from actual measurement reading interval and (b) monthly average values of the SSM.

Preprints (www.preprints.org) | NOT PEER-REVIEWED | Posted: 6 September 2023 doi:10.20944/preprints202309.0289.v1

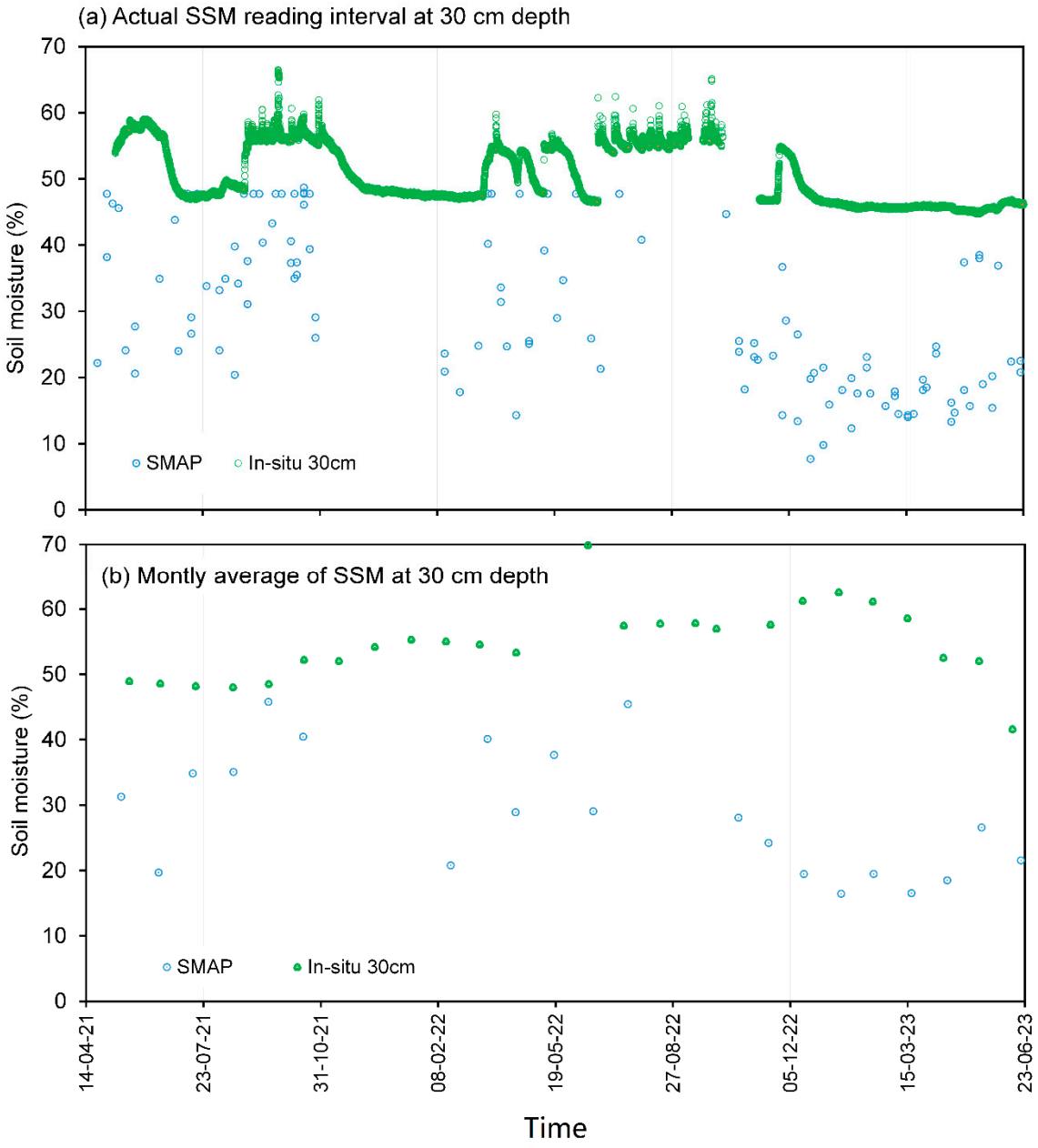

Figure 9. Variations of SMAP and in-situ soil moisture (30 cm depth) from Station VLGE49: (a) from actual measurement reading interval and (b) monthly average values of the SSM.

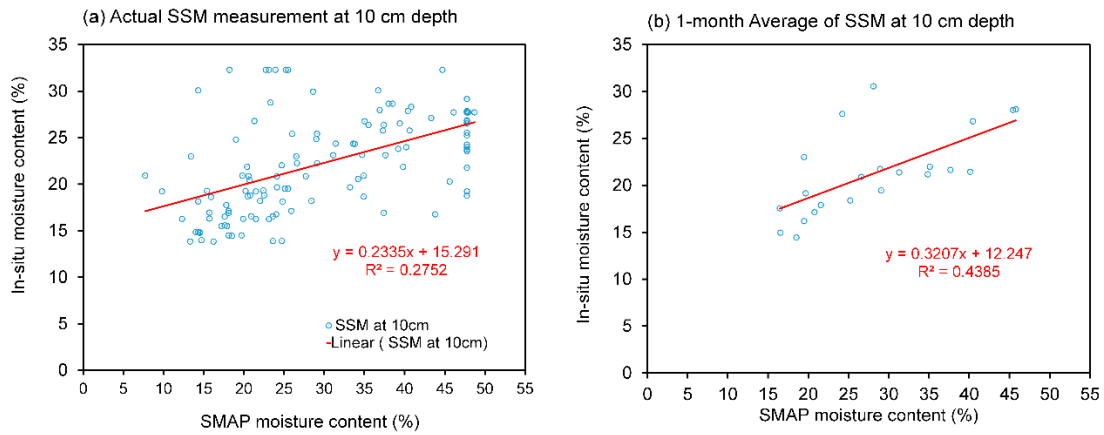

Preprints (www.preprints.org) | NOT PEER-REVIEWED | Posted: 6 September 2023 doi:10.20944/preprints202309.0289.v1

Figure 10. Correlation between of SMAP and in-situ soil moisture (10 cm depth) for Station VLGE49: (a) using soil moisture actual measurement reading time and (b) monthly average of the SSM.

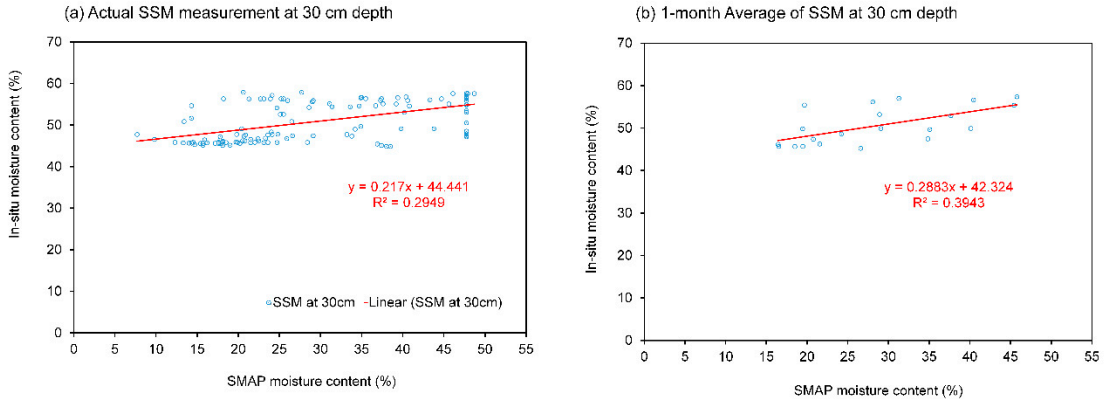

Figure 11. Correlation between of SMAP and in-situ soil moisture (30 cm depth) for Station VLGE49: (a) using soil moisture actual measurement reading time and (b) monthly average of the SSM.

3.4.2. Linear correlation coefficients and soil properties

The correlation between SSM and in-situ soil moisture based on 1-month average values can be expressed using linear equation in the following.

$$\theta = M \bullet SSM + C \quad (5)$$

This correlation was determined for all ten telemetry stations and the fitting parameters (M,C) are summarized in Tables 6 and 7 together with the coefficient of determination (R^2). For three station (KKCN, PAII and SWR036), the correlations were unreliable, both due to excessive fluctuation in SMAP data and malfunctions in the in-situ moisture sensors. The correlation coefficients are not present for these stations. Among the other seven stations, the coefficient of determinations range between 0.13 to 0.58 which show a varying degree of fitting. The relatively poor fitting between the SMAP soil moisture and in-situ measurement is expected to be related to the disproportionate measurement areas which will be discussed in the next section. The slope (M) of the linear equation are mostly below unity, which suggest that the SSM varied with less amplitude than the in-situ soil moisture. The intercept (C) are also greater than zero for all cases, indicating that even when SMAP surface moisture tend to zero, some residual water content still remains in the surface soil. This kind of correlation is valuable for site-specific purpose and can be extended to sites with similar conditions.

Table 6. Linear correlation coefficients for monthly SMAP vs in-situ soil moisture Stations 1 to 5.

No.	1	2		3		4	5		
Station	KKCN	VLGE49		HNKA		WGYG	VLGE50		
Depth (cm)	all	10	30	10	100	10	10	30	100
M	NR	0.3207	0.2883	0.2387	0.3428	0.1283	0.364	0.3451	0.2059
C	NR	12.247	42.324	13.493	19.155	42.016	24.438	21.165	29.807
R^2	NR	0.4385	0.3943	0.2086	0.4134	0.1756	0.4971	0.5471	0.5814
NR = Not reliable (negative correlation or $R^2 < 0.1$)									

Table 7. Linear correlation coefficients for monthly SMAP vs in-situ soil moisture Stations 6 to 10.

No	6			7	8				9		10
Station	NMUB			PAII	BNKE				THAT		SWR036
Depth (cm)	10	30	60	all	10	30	60	100	30	100	all
M	0.4217	1.1006	0.9325	NR	0.4748	0.6607	0.3699	0.3497	0.255	0.3873	NR

Preprints (www.preprints.org) | NOT PEER-REVIEWED | Posted: 6 September 2023 doi:10.20944/preprints202309.0289.v1

C	21.306 1.5069	0.4633	NR	9.0514	2.7021	12.625	21.448	5.6962	4.0059	NR
R^2	0.1296 0.5333	0.5378	NR	0.5247	0.6376	0.4906	0.4722	0.2969	0.3345	NR

NR = Not reliable (negative correlation or $R^2 < 0.1$)

The values of M and C are further correlated to soil's physical properties ($X_1, ...X_7$) as explained in Section 3.1. The multiple linear regressions for M and C can be expressed in Equation (6) and (7) respectively,

$$M = D + a_1X_1 + a_2X_2 + a_3X_3 + a_4X_4 + a_5X_5 + a_6X_6 + a_7X_7 \quad (6)$$

$$C = E + b_1X_1 + b_2X_2 + b_3X_3 + b_4X_4 + b_5X_5 + b_6X_6 + b_7X_7 \quad (7)$$

Where D, a_i , and b_i (i = 1,2,3,..,7) are curve fitting parameters obtained from regression analysis as summarized in Table 6. The coefficient of determination (R^2) from the multiple linear regression analysis of M parameter and C parameter was 0.933 and 0.847 respectively. Provided that basic soil properties ($X_1, ...X_7$) are known at the site, the in-situ soil moisture can then be predicted using SMAP soil moisture and Equations (5) to (7). The estimated parameters given by the regression are summarized in Table 8.

Table 8. Multiple linear regression coefficients for predicting the sensor calibration equations using soil properties.

D	**a_1**	**a_2**	**a_3**	**a_4**	**a_5**	**a_6**	**a_7**
–400.298	–0.00987	4.0132	4.0052	4.0042	4.0083	0.1167	0.0006060
E	**b_1**	**b_2**	**b_3**	**b_4**	**b_5**	**b_6**	**b_7**
–219718.912	0.083	2196.216	2197.531	2198.317	2197.613	–54.224	0.377

3.4.3. Upscaling of SMAP, in-situ soil moistures and validation for croplands

As discussed earlier, the relatively poor correlation between the SMAP soil moisture and in-situ soil moisture at any specific telemetry station was largely attributed to the disproportionate measurement areas (1 sq.km for the SMAP soil moisture versus 0.01sq.m for the in-situ soil moisture) as well as spatial and temporal variation of in-situ soil moisture. Land cover types have also been shown to play a significant role in the correlation between the two kinds of measurement. Croplands generally demonstrated a better correlation due to the more uniformity of the landcover and thus in-situ soil moisture within the SMAP measurement pixel as compared to other land-covers. In this study, the MODIS land-cover type product obtained from International Geosphere-Biosphere Program (IGBP) was used to classify the telemetry station in each SMAP measurement pixel. Seven stations are located in the croplands, namely PAII, VLGE49, BNKE, THAT, VLGE50, WGYS, and HNKA, while Station NMUB is in the woody savannas, SWR036 is in the evergreen broadleaf forests, and KKCN falls within the grassland type. Only data from seven stations in the croplands were used in further analysis. The average value of soil moistures from all seven stations in the croplands were used in order to upscale both SMAP and in-situ soil moistures, thus generalizing the soil moisture to represent the climate regimes of the cropland regions in Thailand.

In Figure 12, the variation of average SMAP moistures obtained from the seven measurement pixels in croplands (representing all seven telemetry stations), are depicted from the period between 2017 and 2022. These SMAP moistures were calculated using 3-month running average approach. The method aligns with the averaging period of the Oceanic Niño Index (ONI), which is also displayed in the figure. The Oceanic Niño Index (ONI) is NOAA's primary index for tracking the ocean part of ENSO, the El Niño-Southern Oscillation climate pattern that indicates the difference from average—in the surface waters of the east-central tropical Pacific. Also shown in the figure are the periods of El Niño (ONI $\geq$ 0.5) and La Niña (ONI $\leq$ 0.5). The average SMAP moisture calculated using the seasonal mean approach are also shown for comparison. The episodes of La Niña in 2018, 2021 and 2022 (shown as blue bar charts) contributed to the increase in soil moisture in these years,

Preprints (www.preprints.org) | NOT PEER-REVIEWED | Posted: 6 September 2023 doi:10.20944/preprints202309.0289.v1

while the El Niño in 2019 (red bar charts) gave rise to decrease in the soil moisture. The rainy season SMAP moisture reached the maximum value of 0.42 in 2022 (La Niña), while the minimum dry season SMAP moisture was 0.22 in 2020 (one year after El Niño).

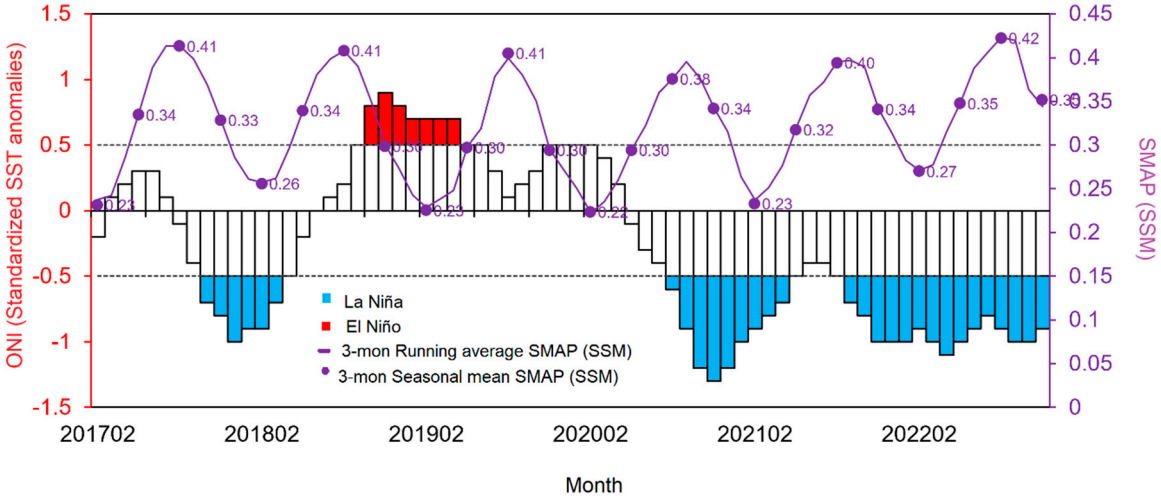

Figure 12. Average SMAP surface soil moisture from cropland areas and ONI index.

Based on the findings that the three-month running average period resulted in a satisfactory agreement between the soil moisture and Oceanic Niño Index (ONI), this averaging approach was adopted to determine the correlation between in-situ and SMAP soil moisture (SSM) data. The study utilized in-situ soil moisture data collected from seven stations situated in croplands. The data was averaged both spatially, between seven stations, and temporally, considering the three-month running period spanning from 2021 to 2022. Figure 13 shows the relationship between the average SSM and in-situ water content,θ, at depths of 10 and 30cm. The data was fitted using a linear model, yielding R-squared values ranging from 0.83 to 0.87, indicating a strong correlation between SSM and in-situ θ when averaged using such approach. At a depth of 10cm, the correlation revealed a systematic transformation shift of approximately –3%, suggesting that SSM tended to over-predict in-situ moisture (θ). However, the slope of the linear equation remained close to 1, indicating a relatively consistent relationship. Similarly, at 30cm depth, the correlation indicated SSM's tendency to over-predict in-situ θ, with a slope of the linear equation measuring approximately 0.53.

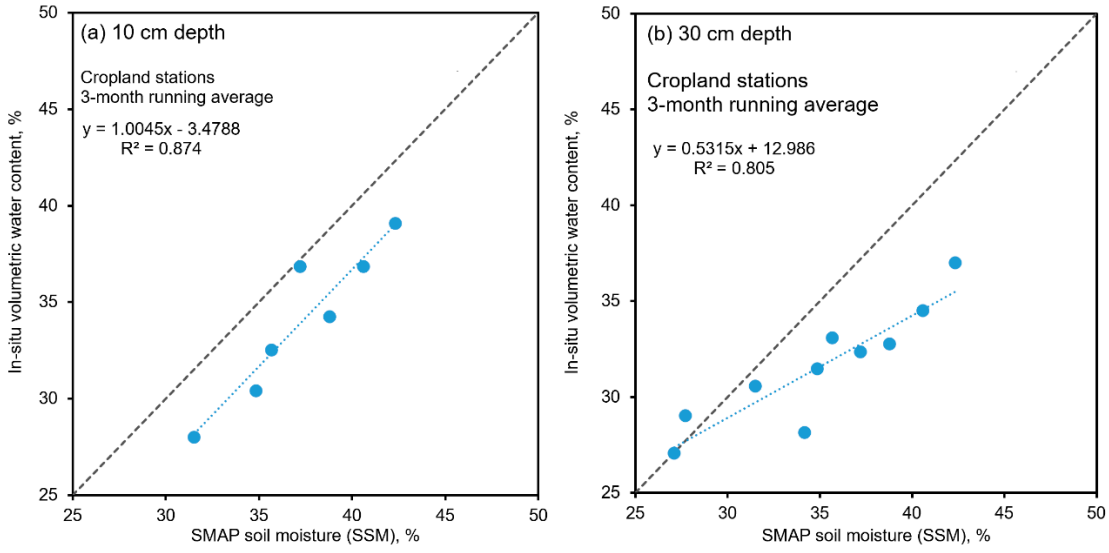

Preprints (www.preprints.org) | NOT PEER-REVIEWED | Posted: 6 September 2023 doi:10.20944/preprints202309.0289.v1

Figure 13. Relationships between SMAP soil moisture (SSM) and in-situ volumetric water content, using data averaged between 7 stations in Cropland, and averaged for each three-month running period spanning from 2021 to 2022.

One of the objectives of this research project was to produce a monthly surface soil moisture data, to be used for climate modelling and improving weather forecast in a national scale. The linear models presented earlier in Figure 13 using the three-month running average and Cropland data, were then utilized to adjust the original monthly SMAP data to be more accurate and suitable for Thailand's specific conditions. However, it is essential to acknowledge that extending the model calibrated with Cropland data to all land cover types in the country might introduce some inherent errors.

To assess the effectiveness of the SSM adjustment, we compared monthly SMAP soil moistures with and without model adjustment against one-month average in-situ soil moisture (θ_{month}) from ten telemetry stations between January and May 2023, as shown in Figure 14. We calculated the root mean square errors (RMSE) to demonstrate the correlation improvements that could be expected from the SMAP SSM adjustment. For the case of 10 cm deep in-situ soil moisture, the linear model adjustment of SMAP SSM did not significantly improve the accuracy of the correlation. The RMSE values were comparable, measuring 0.021 and 0.020 for the adjusted and original SMAP SSMs, respectively (Fig. 14a).

However, a promising trend was observed for the adjusted SAMP SSM at the depth of 30 cm (Fig. 14b). The RMSE value decreased from 0.026 for the original SMAP SSM to 0.018 after adjustment. This suggests that the adjustment technique holds potential for enhancing accuracy at greater soil depths. Overall, while the linear model adjustment of SMAP SSM showed mixed results, it has demonstrated the ability to improve the correlation in certain scenarios, particularly at greater soil depths. Further investigation and refinement of the models might be necessary to enhance the accuracy of surface soil moisture data across various land cover types in Thailand.

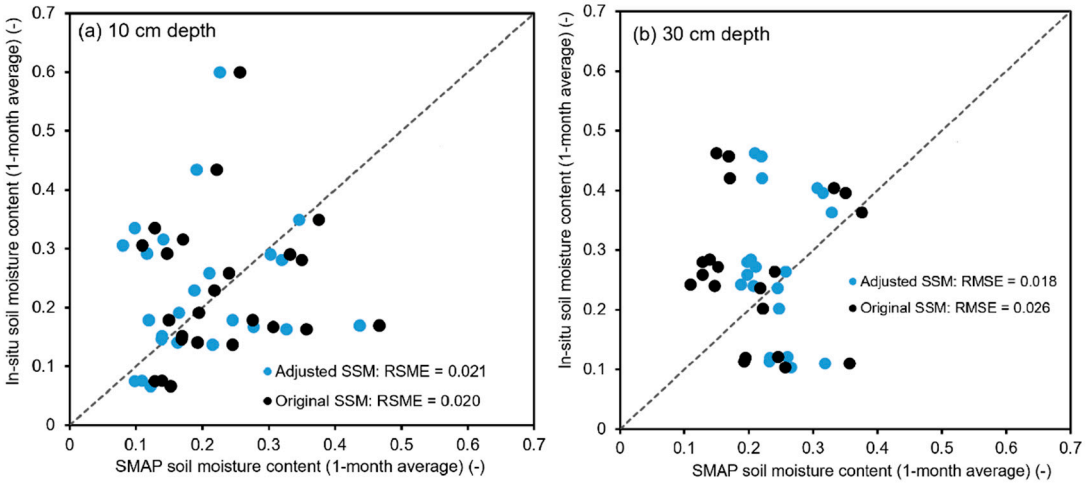

Figure 14. Relationships between 1-month average original and adjusted SMAP soil moisture (SSM) and in-situ volumetric water content, for all 10 stations: a) at 10 cm depth and b) at 30 cm depth.

4. Discussion and Conclusions

The present study undertakes an in-depth exploration of the intricate interplay between remotely sensed SMAP data and in-situ soil moisture measurements, with the overarching goal of advancing our comprehension of soil moisture dynamics. This multifaceted investigation encompasses an array of aspects, including temporal variations, correlation coefficients, and the impact of soil properties. Collectively, these facets contribute to a comprehensive understanding of the complex process of soil moisture estimation.

 doi:10.20944/preprints202309.0289.v1

One of the central considerations in this study revolves around addressing the temporal variation discrepancies between SMAP data and in-situ measurements spanning the years 2021 to 2023. This discrepancy stems from the inherent differences in temporal resolutions between the two datasets. The solution lies in employing a monthly averaging approach, which serves to attenuate the inherent fluctuations in soil moisture and thus enhance the reliability of the correlation analysis. The observed disparities in soil moisture variations underscore the multifaceted nature of soil moisture dynamics. Interestingly, SMAP soil moisture exhibits more pronounced amplitude variations compared to in-situ readings. A noteworthy phenomenon arises when in-situ measurements surpass SSM readings at greater soil depths, offering intriguing insights into the underlying influences, including soil properties, groundwater interactions, and spatial variations. The introduction of a 1-month averaging scheme effectively highlights the potential of this approach to mitigate these discrepancies, resulting in a smoother soil moisture variation profile and subsequently improving the correlation between SMAP data and in-situ measurements.

A significant focus of this study lies in exploring the linear correlation coefficients, characterized by the coefficients M and C. While some stations exhibit unreliable correlations due to factors such as SMAP data volatility and sensor malfunctions, the reliable correlations provide valuable insights into understanding soil moisture dynamics. The diverse range of calculated correlation coefficients, as indicated by the coefficient of determination (R^2), underscores the importance of considering the proportionality of measurement areas. Although these correlations are specific to individual stations, their implications extend to site-specific applications and analogous conditions, emphasizing the versatility of remote sensing data.

Furthermore, the integration of essential soil properties into the correlation analysis through multiple linear regression enhances the scientific rigor of this study. This analytical approach illuminates the intricate interconnections between soil characteristics and moisture measurements, revealing the multifaceted nature of soil-water interactions. The resulting regression equations establish crucial relationships between linear coefficients (M and C) and soil properties (X1, ..., X7), thereby shedding light on the underlying mechanisms governing correlations. This enriches the predictive potential of in-situ soil moisture using SMAP data, particularly in cases where soil property information is limited.

The imperative of upscaling and correlating soil moisture data from diverse sources, such as satellite-based SMAP measurements and in-situ observations, underscores the need for a comprehensive understanding of soil moisture dynamics across various scales. The insights gained from this study highlight the pivotal role of measurement area proportions and land cover types in influencing correlation outcomes. The distinct scales of measurement between SMAP soil moisture and in-situ data, combined with the inherent variations in in-situ measurements, impact correlation results. The role of land cover type emerges as a significant factor, with croplands displaying enhanced correlations due to their uniformity. Utilizing MODIS land cover type data allows for effective classification of telemetry stations, providing insights into the role of land cover in determining correlation efficacy.

Temporal averaging emerges as a key technique in bridging the temporal gap between SMAP data and high-frequency in-situ measurements. The alignment of the three-month running average with the Oceanic Niño Index (ONI) period results in a meaningful agreement between soil moisture patterns and climate oscillations. Extending this approach to correlate SMAP and in-situ soil moisture data proves effective, particularly when focusing on cropland regions. Through spatial and temporal averaging, robust correlations are achieved, harmonizing diverse data sources into a coherent relationship.

The correlation analysis further uncovers significant insights into the interrelation between SMAP soil moisture (SSM) and in-situ water content (θ) at varying depths. By utilizing linear regression models, correlations are established for average SSM and in-situ θ at depths of 10 cm and 30 cm. The high R-squared values, ranging from 0.83 to 0.87, underline the strong correlations achieved through the three-month running average approach. Notably, distinct patterns emerge from this analysis. At a depth of 10 cm, SSM consistently exhibits a slight tendency to slightly over-predict

 doi:10.20944/preprints202309.0289.v1

in-situ moisture (θ), with a systematic transformation shift of around –3%. Importantly, the linear equation's slope remains close to unity, indicating a proportional correlation. Similarly, at a 30 cm depth, the correlation highlights SSM's consistent inclination to over-predict in-situ θ, with a slope of the linear equation around 0.53.

While the adjustments we explored did not consistently yield significant improvements in all cases, the positive outcomes observed, particularly for greater soil depths, point towards the potential for refining our models. These results highlight the intricate nature of soil moisture dynamics in diverse land cover types, emphasizing the importance of tailored approaches for calibration and adjustment. In our endeavor to create accurate soil moisture data for climate modeling and weather prediction, this study offers valuable insights and suggests directions for future research. It is clear that the linear adjustment method has promise, but its effectiveness depends on intricate relationships that require further investigation and validation. These endeavors have the potential to deepen our understanding of soil moisture behavior, contributing to more precise and dependable environmental modeling and predictive systems.

In conclusion, this study signifies a significant advancement in refining soil moisture estimation by bridging the gap between remote sensing and in-situ measurements. The investigation into temporal variations, correlation coefficients, and the role of soil properties culminate in a comprehensive understanding of soil moisture dynamics. The study underscores the crucial role of temporal averaging and the impact of land cover types in unraveling the complexities of correlation patterns.

List of Notations

SMAP	Soil Moisture Active/Passive
θ	In-situ volumetric water content
SSM	Surface soil moisture
V_w	Volume of soil water
V	Total volume of soil
x	Sensor reading (mA)
$a,\ b$	Fitting parameters for water content-voltage sensor calibration from linear regression
$\alpha_c,\ \alpha_1,.,\alpha_7$	Multiple linear regression parameters for sensor calibration based on physical properties for a
$\beta_c,\ \beta_1,.,\beta_7$	Multiple linear regressions parameters for sensor calibration based on physical properties for b
$X_1,.,X_7$	Soil's physical properties used in multiple linear regressions
θ_s	Saturated volumetric water content
θ_r	Residual volumetric water content
s	Soil's suction
p, m, n	Van Genuchten's fitting parameter for soil-water retention curve
M, C values	Linear regression fitting parameters between θ and SSM based on 1-month average
$D,\ a_1,..\ a_7$	Multiple linear regression parameters for M based on physical properties
$E, b_1, \ldots, b_7$	Multiple linear regression parameters for C based on physical properties

Author Contributions: Conceptualization and methodology, K.T. S.S. and A.J.; validation, A.J. and S.S.; formal analysis, A.J. S.S; data curation, A.J., S.S., K.S., N.T., R.S., A.F.., P.P., J.A.; writing—original draft preparation, A.J. and S.S.; writing—review and editing, K.T. All authors have read and agreed to the published version of the manuscript.

Funding: This study was financially supported by the Thailand Science Research and Innovation (TSRI) under Fundamental Fund No. 48873, No. 160399 and No. 180529 under "Sub-Seasonal to Seasonal (S2S) Prediction Project for Disaster Risk Reduction and Water Management in Thailand (S2S Thailand Project)".

Institutional Review Board Statement: Not applicable.

Informed Consent Statement: Not applicable.

Data Availability Statement: Reader can find data availability of the SMAP soil moisture via https://smap.jpl.nasa.gov/ (Last Accessed: 13 June 2023). For in-situ soil moisture data over Thailand, they can be found by contacting corresponding author.

Acknowledgments: The authors express their sincere gratitude to the Hydro-informatics Institute, Thailand, for their generous support in facilitating the installation of in-situ soil moisture sensors into their telemetry system. Additionally, the authors gratefully acknowledge the NASA Jet Propulsion Laboratory, California Institute of Technology, for providing valuable access to SMAP soil moisture availability.

Conflicts of Interest: The authors declare no conflict of interest.

References

1. Korres, W.; Reichenau, T.G.; Fiener, P.; Koyama, C.N.; Bogena, H.R.; Cornelissen, T.; Baatz, R.; Herbst, M.; Diekkrüger, B.; Vereecken, H,; Schneider, K. Spatio-temporal soil moisture patterns – A meta-analysis using plot to catchment scale data. *Journal of Hydrology* **2015**, *520*, pp. 326-341.
2. Mohanty, B.P.; Cosh, M.; Lakshmi, V.; Montzka, C. Soil Moisture Remote Sensing State-Of-The-Science. *Vadose Zone J.* **2017**, 16, pp. 1-9.
3. Entekhabi, D.; Njoku, E.G.; O'Neill, P.E.; Kellogg, K.H.; Crow, W.T.; Edelstein, W.N.; Entin, J.K.; Goodman, S.D.; Jackson, T.J.; Johnson, J.; et al. The Soil Moisture Active Passive (SMAP) mission. *Proc. IEEE.* **2010,** *98*, pp. 704–716.
4. Forgotson, C.; O'Neill, P.E.; Carrera, M.L.; Bélair, S.; Das, N.N.; Mladenova. I.E.; Bolten, J.D.; Jacobs, J.M.; Cho, E.; Escobar, V.M. How Satellite Soil Moisture Data Can Help to Monitor the Impacts of Climate Change: SMAP Case Studies. *IEEE Journal of Selected Topics in Applied Earth Observations and Remote Sensing* **2020**, *13*, pp. 1590-1596.
5. Rahman, M.S.; Di, L.; Yu, E.; Lin, L.; Zhang, C.; Tang, J. Rapid Flood Progress Monitoring in Cropland with NASA SMAP. *Remote Sens*. **2019**, 11(2), pp. 191; https://doi.org/10.3390/rs11020191
6. Zhang, X.; Zhang, T.; Zhou, P.; Shao, Y.; Gao, S. Validation Analysis of SMAP and AMSR2 Soil Moisture Products over the United States Using Ground-Based Measurements. *Remote Sens.* **2017**, 9(2), 104; https://doi.org/10.3390/rs9020104
7. Das, N., D. Entekhabi, R. S. Dunbar, S. Kim, S. Yueh, A. Colliander, P. E. O'Neill, T. Jackson, T. Jagdhuber, F. Chen, W. T. Crow, J. Walker, A. Berg, D. Bosch, T. Caldwell, and M. Cosh. **2020**. SMAP/Sentinel-1 L2 Radiometer/Radar 30-Second Scene 3 km EASE-Grid Soil Moisture, Version 3. Boulder, Colorado USA. NASA National Snow and Ice Data Center Distributed. https://doi.org/10.5067/ASB0EQO2LYJV.
8. Das, N., D. Entekhabi, S. Dunbar, J. Chaubell, A. Colliander, S. Yueh, T. Jagdhuber, F. Chen, W. T. Crow, P. E. O'Neill, J. Walker, A. Berg, D. Bosch, T. Caldwell, M. Cosh, C. H. Collins, E. Lopez-Baeza, and M. Thibeault. **2019**. The SMAP and Copernicus Sentinel 1A/B microwave active-passive high-resolution surface soil moisture product, Remote Sensing of Environment. 233. 111380. https://doi.org/10.1016/j.rse.2019.111380
9. Suwansawat, S.; Benson, C. H. Cell size for water content-dielectric constant calibrations for time domain reflectometry. *Geotechnical Testing Journal*, **1999,** *22(1)*, 3-12. doi:10.1520/gtj11311j
10. Barus, R. M. N.; Jotisankasa, A.; Chaiprakaikeow, S.; Sawangsuriya, A. Laboratory and field evaluation of modulus-suction-moisture relationship for a silty sand subgrade. **2019**. *Transportation Geotechnics.* 19, 126-134. doi.org/10.1016/j.trgeo.2019.03.005
11. Shrestha, A.; Jotisankasa, A.; Chaiprakaikeow, S.; Pramusandi, S.; Soralump, S.; Nishimura, S. Determining shrinkage cracks based on the small-strain shear modulus–suction relationship. *Geosciences* **2019**, 9(9), 362; doi:10.3390/geosciences9090362
12. ASTM. Standard test method for permeability of granular soils (constant head). ASTM standard D2434-68. **2006**. *American Society for Testing and Materials*, West Conshohocken, Pa.
13. ASTM. Standard test method for Determination of Thermal Conductivity of Soil and Soft Rock by Thermal Needle Probe Procedure. ASTM standard D 5334 – 00 **2004**. American Society for Testing and Materials, West Conshohocken, Pa.

14. ASTM. Standard Test Methods for Particle-Size Distribution (Gradation) of Soils Using Sieve Analysis. ASTM standard D6913-04. **2009**. American Society for Testing and Materials, West Conshohocken, Pa.
15. ASTM. Standard Test Methods for Liquid Limit, Plastic Limit, and Plasticity Index of Soils. ASTM standard D4318-17. **2018**. American Society for Testing and Materials, West Conshohocken, Pa.
16. ASTM. Standard Test Methods for Specific Gravity of Soil Solids by Water Pycnometer. ASTM standard D854-14. **2016.** American Society for Testing and Materials, West Conshohocken, Pa.
17. Walkley, A.; Black, I. A. An Examination of Degtjareff Method for Determining Soil Organic Matter and a Proposed Modification of the Chronic Acid Titration Method. **1934**. *Soil Science* 37: 29–38. doi:10.1097/00010694-193401000-00003.
18. Brandon, T.; Mitchell, J. Factors influencing thermal resistivity of sands. **1989**. *J. Geotech. Eng.* 115 (12), 1683-1698.
19. Van Genuchten, M.T. A Closed Form Equation for Predicting the Hydraulic Conductivity of Unsaturated Soils. **1980**. *Soil Science Society of America Journal*, 44, 892-898.